

MaskViT: Masked Visual Pre-Training for Video Prediction

Agrim Gupta¹

Stephen Tian¹

Yunzhi Zhang¹

Jiajun Wu¹

Roberto Martín-Martín^{2,1} Li Fei-Fei¹

¹ Stanford University, ² Salesforce AI

Abstract: The ability to predict future visual observations conditioned on past observations and motor commands can enable embodied agents to plan solutions to a variety of tasks in complex environments. This work shows that we can create good video prediction models by pre-training transformers via masked visual modeling. Our approach, named MaskViT, is based on two simple design decisions. First, for memory and training efficiency, we use two types of window attention: spatial and spatiotemporal. Second, during training, we mask a *variable* percentage of tokens instead of a *fixed* mask ratio. For inference, MaskViT generates all tokens via iterative refinement where we incrementally decrease the masking ratio following a mask scheduling function. On several datasets we demonstrate that MaskViT outperforms prior works in video prediction, is parameter efficient, and can generate high-resolution videos (256×256). Further, we demonstrate the benefits of inference speedup (up to $512\times$) due to iterative decoding by using MaskViT for planning on a real robot. Our work suggests that we can endow embodied agents with powerful predictive models by leveraging the general framework of masked visual modeling with minimal domain knowledge.

1 Introduction

Evidence from neuroscience suggests that human cognitive and perceptual capabilities are supported by a predictive mechanism to anticipate future events and sensory signals [1, 2]. Such a mental model of the world can be used to simulate, evaluate, and select among different possible actions. This process is fast and accurate, even under the computational limitations of biological brains [3]. Endowing robots with similar predictive capabilities would allow them to plan solutions to multiple tasks in complex and dynamic environments, e.g., via visual model-predictive control [4–6].

Predicting visual observations for embodied agents is however challenging and computationally demanding: the model needs to capture the complexity and inherent stochasticity of future events while maintaining an inference speed that supports the robot’s actions. Therefore, recent advances in autoregressive generative models, which leverage Transformers [7] for building neural architectures and learn good representations via self-supervised generative pretraining [8], have not benefited video prediction or robotic applications. We in particular identify three technical challenges. First, memory requirements for the full attention mechanism in Transformers scale quadratically with the length of the input sequence, leading to prohibitively large costs for videos. Second, there is an inconsistency between the video prediction task and autoregressive masked visual pretraining – while the training process assumes *partial* knowledge of the ground truth future frames, at test time the model has to predict a complete sequence of future frames from *scratch*, leading to poor video prediction quality. Third, the common autoregressive paradigm effective in other domains would be too slow for robotic applications.

To address these challenges, we present **Masked Video Transformers** (MaskViT): a simple, effective and scalable method for video prediction based on masked visual modeling. Since using pixels

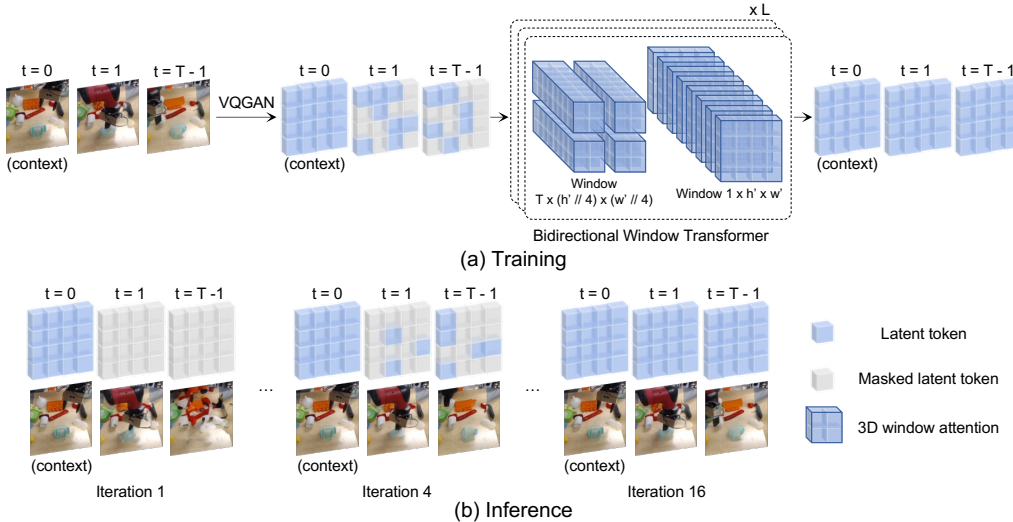


Figure 1: **MaskViT.** (a) Training: We first encode the video frames into latent codes via VQ-GAN. A *variable* number of tokens in future frames are masked, and the network is trained to predict the masked tokens. A block in MaskViT consists of two layers with window-restricted attention: spatial and spatiotemporal. (b) Inference: Videos are generated via iterative refinement where we incrementally decrease the masking ratio following a mask scheduling function. Videos available at [this project page](#).

directly as frame tokens would require an inordinate amount of memory, we use a discrete variational autoencoder (dVAE) [9, 10] that compresses frames into a smaller grid of visual tokens. We opt for compression in the spatial (image) domain instead of the spatiotemporal domain (videos), as preserving the correspondence between each original and tokenized video frame allows for flexible conditioning on any subset of frames – initial (past), final (goal), and possibly equally spaced intermediate frames. However, despite operating on tokens, representing 16 frames at 256 tokens per frame still requires 4,096 tokens, incurring prohibitive memory requirements for full attention. Hence, to further reduce memory, MaskViT is composed of alternating transformer layers with non-overlapping *window-restricted* [7] spatial and spatiotemporal attention.

To reduce the inconsistency between the masked pretraining and the video prediction task and to speed up inference, we take inspiration from non-autoregressive, iterative decoding methods in generative algorithms from other domains [11–15]. We propose a novel iterative decoding scheme for videos based on a mask scheduling function that specifies, during inference, the number of tokens to be decoded and kept at each iteration. A few initial tokens are predicted over multiple initial iterations, and then the majority of the remaining tokens can be predicted rapidly over the final few iterations. This brings us closer to the ultimate video prediction task, where only the first frame is known and all tokens for other frames must be inferred. Our proposed prediction procedure provides fast predictions without temporally increasing quality degradation due to its iterative non-autoregressive nature. To further close the training-test gap, during training we mask a *variable* percentage of tokens, instead of using a *fixed* masking ratio. This simulates the different masking ratios MaskViT will encounter during iterative decoding in the actual video prediction task.

Through experiments on several publicly available real-world video prediction datasets [16–18], we demonstrate that MaskViT achieves competitive or state-of-the-art results in a variety of metrics. Moreover, MaskViT can predict considerably higher resolution videos (256×256) than previous methods. More importantly, thanks to iterative decoding, MaskViT is up to $512\times$ faster than autoregressive methods, enabling its application for planning on a real robot (§ 4.4). These results indicate that we can endow embodied agents with powerful predictive models by leveraging the advances in self-supervised learning in language and vision, without engineering domain-specific solutions.

2 Related Work

Video prediction. The video prediction task refers to the problem of generating videos conditioned on past frames [19, 20], possibly with an additional natural language description [21–24] and/or motor commands [25–28]. Multiple classes of generative models have been utilized to tackle this problem, such as Generative adversarial networks (GANs) [29–31], Variational Autoencoders (VAEs) [26–28, 32–35], invertible networks [36], autoregressive [37–39] and diffusion [40, 41] models. Our work focuses on predicting future frames conditioned on past frames or motor commands and belongs to the family of two-stage methods that first encode the videos into a downsampled latent space and then use transformers to model an autoregressive prior [37, 38]. A common drawback of these methods is the large inference time due to autoregressive generation. MaskViT overcomes this issue by using an iterative decoding scheme, which significantly reduces inference time.

Masked autoencoders. Masked autoencoders are a type of denoising autoencoder [42] that learn representations by (re)generating the original input from corrupted (i.e., masked) inputs. Masked language modeling was first proposed in BERT [8] and has revolutionized the field of natural language processing, especially when scaled to large datasets and model sizes [43, 44]. The success in NLP has also been replicated in vision by masking patches of pixels [45, 46] or masking tokens generated by a pretrained dVAE [47, 48]. Recently, these works have also been extended to video domains to learn good representations for action recognition [49, 50]. Unlike them, we apply masked visual modeling for video prediction, and we use a *variable* masking ratio during training to reduce the difference between masked pretraining and video prediction. Another related line of work is leveraging good visual representations learnt via self supervised learning methods [51–53] including masked autoencoders [54] for motor control.

3 MaskViT: Masked Video Transformer

MaskViT is the result of a two-stage training procedure [9, 55]: First, we learn an encoding of the visual data that discretizes images into tokens based on a discrete variational autoencoder (dVAE). Next, we deviate from the common autoregressive training objective and pre-train a bidirectional transformer with window-restricted attention via *masked visual modeling* (MVM). In the following section, we describe our image tokenizer, bidirectional transformer, masked visual pre-training, and iterative decoding procedure.

3.1 Learning Visual Tokens

Videos contain too many pixels to be used directly as tokens in a transformer architecture. Hence, to reduce dimensionality, we first train a VQ-VAE [9] for individual video frames so that we can represent videos as sequences of grids of discrete tokens. VQ-VAE consists of an encoder $E(x)$ that encodes an input image $x \in \mathbb{R}^{H \times W \times 3}$ into a series of latent vectors. The vectors are discretized through a nearest neighbour look up in a codebook of quantized embeddings, $\mathcal{Z} = \{z_k\}_{k=1}^K \subset \mathbb{R}^{n_z}$. A decoder D is trained to predict a reconstruction of the image, \hat{x} , from the quantized encodings. In our work, we leverage VQ-GAN [10], which improves upon VQ-VAE by adding adversarial [56] and perceptual losses [57, 58]. Each video frame is individually tokenized into a 16×16 grid of tokens, regardless of their original resolution (Fig. 1, a, left). Instead of using 3D extensions of VQ-VAE which perform spatiotemporal compression of videos [37], our per-frame compression enables us to condition on arbitrary context frames: initial, final, and possibly intermediate ones.

3.2 Masked Visual Modeling (MVM)

Inspired by the success of masked language [8] and image [47, 45] modeling, and in the spirit of unifying methodologies across domains, we pre-train MaskViT via MVM for video prediction. Our pre-training task and masking strategy are straightforward: we keep the latent codes corresponding to context frames intact and mask a random number of tokens corresponding to future frames. The network is trained to predict masked latent codes conditioned on the unmasked latent codes.

Concretely, we assume access to input context frames for T_c time steps, and our goal is to predict T_p frames during test time. We first quantize the entire video sequence into latent codes $Z \in \mathbb{R}^{T \times h \times w}$. Let $Z_p = [z_i]_{i=1}^N$ denote the latent tokens corresponding to future video frames, where $N = T_p \times h \times w$. Unlike prior work on MVM [47, 45] that uses a *fixed* masking ratio, we propose to use a *variable* masking ratio that reduces the gap between pre-training task and inference leading to better evaluation results (see § 3.4). Specifically, during training, for each video in a batch, we first select a masking ratio $r \in [0.5, 1)$ and then randomly select and replace $\lfloor r \cdot N \rfloor$ tokens in Z_p with a [MASK] token. The pre-training objective is to minimize the negative log-likelihood of the visual tokens given the masked video as input: $\mathcal{L}_{\text{MVM}} = - \mathbb{E}_{x \in \mathcal{D}} \left[\sum_{\forall i \in N^M} \log p(z_i | Z_p^M, Z_c) \right]$, where \mathcal{D} is the training dataset, N^M represents randomly masked positions, and Z_p^M denotes the output of applying the mask to Z_p , and Z_c are latent tokens corresponding to context frames. The MVM training objective is different from the causal autoregressive training objective as the conditional dependence is *bidirectional*: *all* masked tokens are predicted conditioned on *all* unmasked tokens.

3.3 Bidirectional Window Transformer

Transformer models composed entirely of global self-attention modules incur significant compute and memory costs, especially for video tasks. To achieve more efficient modeling, we propose to compute self-attention in windows, based on two types of non-overlapping configurations: 1) Spatial Window (SW): attention is restricted to all the tokens within a subframe of size $1 \times h \times w$ (the first dimension is time); 2) Spatiotemporal Window (STW): attention is restricted within a 3D window of size $T \times h' \times w'$. We sequentially stack the two types of window configurations to gain both *local* and *global* interactions in a single block (Fig. 1, a, center) that we repeat L times. Surprisingly, we find that a small window size of $h' = w' = 4$ is sufficient to learn a good video prediction model while significantly reducing memory requirements (Table 2b). Note that our proposed block enjoys global interaction capabilities without requiring padding or cyclic-shifting like prior works [59, 60], nor developing custom CUDA kernels for sparse attention [61] as both window configurations can be instantiated via simple tensor reshaping.

3.4 Iterative Decoding

Decoding tokens autoregressively during inference is time-consuming, as the process scales linearly with the number of tokens, and this can be prohibitively large (e.g., 4,096 for a video with 16 frames and 256 tokens per frame). Our video prediction training task allows us to predict future video frames via a novel iterative non-autoregressive decoding scheme: inspired by the forward diffusion process in diffusion models [12, 13] and the iterative decoding in generative models [14, 15] we predict videos in T steps where $T \ll N$, the total number of tokens to predict.

Concretely, let $\gamma(t)$, where $t \in \{\frac{0}{T}, \frac{1}{T}, \dots, \frac{T-1}{T}\}$, be a mask scheduling function (Fig. 3) that computes the mask ratio for tokens as a function of the decoding steps. We choose $\gamma(t)$ such that it is monotonically decreasing with respect to t , and it holds that $\gamma(0) \rightarrow 1$ and $\gamma(1) \rightarrow 0$ to ensure that our method converges. At $t = 0$, we start with $Z = [Z_c, Z_p]$ where all the tokens in Z_p are [MASK] tokens. At each decoding iteration, we predict *all* the tokens conditioned on *all* the previously predicted tokens. For the next iteration, we mask out $n = \lceil \gamma(\frac{t}{T})N \rceil$ tokens by keeping all the previously predicted tokens and the most confident token predictions in the current decoding step. We use the softmax probability as our confidence measure.

4 Experimental Evaluation

In this section, we evaluate our method on three different datasets and compare its performance with prior state-of-the-art methods, using four different metrics. We also perform extensive ablation studies of different design choices, and showcase that the speed improvements due to iterative decoding enable real-time planning for robotic manipulation tasks. For qualitative results, see § B.1 and videos on our [project website](#).

RoboNet [18]	param.	FVD↓	PSNR↑	SSIM↑	LPIPS↓	BAIR [16]	param.	FVD↓
SVG [26]	298M	123.2	23.9	87.8	0.060	SV2P [32]	—	262.5
GHVAE [27]	599M	95.2	24.7	89.1	0.036	LVT [38]	—	125.8
FitVid [28]	302M	62.5	28.2	89.3	0.024	SAVP [62]	—	116.4
MaskViT (ours)	257M	133.5	23.2	80.5	0.042	DVD-GAN-FP [29]	—	109.8
MaskViT (ours, 256)	228M	211.7	20.4	67.1	0.170	VideoGPT [37]	—	103.3
KITTI [17]	param.	FVD↓	PSNR↑	SSIM↑	LPIPS↓	TrIVD-GAN-FP [31]	—	103.3
SVG [26]	298M	1217.3	15.0	41.9	0.327	VT [63]	373M	94.0
GHVAE [27]	599M	552.9	15.8	51.2	0.286	FitVid [28]	302M	93.6
FitVid [28]	302M	884.5	17.1	49.1	0.217	MaskViT (ours)	189M	93.7
MaskViT (ours)	181M	401.9	27.2	58.1	0.089	MaskViT (ours, goal cond.)	255M	76.9
MaskViT (ours, 256)	228M	446.1	26.2	40.7	0.270	MaskViT (ours, act cond.)	255M	70.5

Table 1: **Comparison with prior work.** We evaluate MaskViT on BAIR, RoboNet and KITTI datasets. Our method is competitive or outperforms prior work while being more parameter efficient.

blocks	embd. dim	FVD↓	st window	FVD↓	train mem.	train time	mask ratio	FVD↓
6	768	96.6	16 × 4 × 4	96.6	7.0 GB	12.5 hr	0.75	189.3
6	1024	94.2	16 × 8 × 8	93.7	7.9 GB	14.2 hr	0.90	124.1
8	768	99.3	16 × 16 × 16	96.6	11.6 GB	27.9 hr	0.95	110.9
8	1024	99.5	full self attn.	98.2	16.4 GB	40.3 hr	0.98	214.4
							0.5 - 1	96.6

(a) **Model size.** Increasing embedding dim improves FVD.

(b) **Spatiotemporal window size.** Smaller window size is faster, memory efficient, and achieves lower FVD scores.

(c) **Mask ratio.** Variable masking ratio works best.

Table 2: **MaskViT ablation experiments** on BAIR. We compare FVD scores to ablate important design decisions with the default setting: 6 blocks, 768 embedding dimension (embd. dim), 1 × 16 × 16 spatial window, 16 × 4 × 4 spatiotemporal (st) window, and variable masking ratio. Default settings are marked in blue .

4.1 Experimental Setup

Implementation. Our transformer model is a stack of L blocks, where each block consists of two transformer layers with attention restricted to the window size of $1 \times 16 \times 16$ (spatial window) and $T \times 4 \times 4$ (spatiotemporal window), unless otherwise specified. We use learnable positional embeddings, which are the sum of space and time positional embeddings. See § A.1 for architecture details and hyperparameters.

Metrics. We use four evaluation metrics to compare our method with prior work: Fréchet Video Distance (FVD) [64], Peak Signal-to-noise Ratio (PSNR), Structural Similarity Index Measure (SSIM) [65] and Learned Perceptual Image Patch Similarity (LPIPS) [58]. To account for the stochastic nature of video prediction, we follow prior work [28, 26] and report the best SSIM, PSNR, and LPIPS scores over 100 trials for each video. For FVD, we use all 100 with a batch size of 256. We only conducted 1 trial per video for evaluating performance on the BAIR dataset [16].

4.2 Comparison with Prior Work

BAIR. We first evaluate our model on the BAIR robot pushing dataset [16], one of the most studied video modeling datasets. We follow the evaluation protocol of prior works and predict 15 video frames given 1 context frame and no actions. The lack of action conditioning makes this task extremely challenging and tests the model’s ability to predict plausible future robot trajectories and object interactions. MaskViT achieves similar performance to FitVid [28] while being more parameter efficient, and it outperforms all other prior works. In addition, we can easily adapt MaskViT to predict goal-conditioned futures by including the last frame in Z_c . We find that goal conditioning significantly improves performance (approx. 18% FVD improvement). Finally, to predict action-conditioned future frames, we linearly project the action vectors and add them to Z . As expected, action conditioning performs the best, with almost a 25% improvement in FVD.

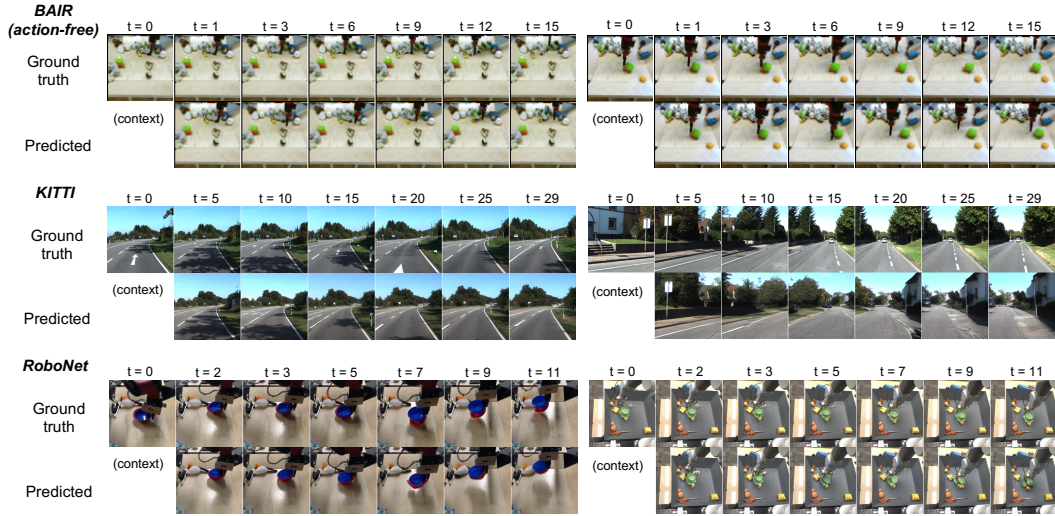


Figure 2: **Qualitative evaluation.** Video prediction results on test set of BAIR (64×64), KITTI (256×256), and RoboNet (256×256). Zoom in for details.

KITTI. The KITTI dataset [17] is a relatively small dataset of 57 training videos. We follow the evaluation protocol of prior work [26] and predict 25 video frames given 5 context frames. Compared to other datasets in our evaluation, KITTI is especially challenging, as it involves dynamic backgrounds, limited training data, and long-horizon predictions. We use color jitter and random cropping data augmentation for training VQ-GAN and do not use any data augmentation for training the second stage. Across all metrics, we find that MaskViT is significantly better than prior works while using fewer parameters. Training a transformer model with full self-attention would require prohibitively large GPU memory due to the long prediction horizon ($30 \times 16 \times 16 = 7680$). However, MaskViT can attend to all tokens because its spatiotemporal windows significantly reduce the size of the attention context. We also report video prediction results for the KITTI dataset at 256×256 resolution, a higher resolution that prior work was not able to obtain.

RoboNet. RoboNet [18] is a large dataset of 15 million video frames of 7 different robotic arms interacting with objects and provides 5 dimensional robot action annotations. We follow the evaluation protocol of prior work [28] and predict 10 video frames given 2 context frames and future actions. At 64×64 resolution, MaskViT is competitive but does not outperform prior works. FVD of the VQ-GAN reconstructions is a lower bound for MaskViT. We found flicker artifacts in the VQ-GAN reconstructions, probably due to our use of per-frame latents, resulting in a high FVD score of 121 for the VQ-GAN reconstructions. MaskViT achieves FVD scores very close to this lower bound but performs worse than prior works due to temporally inconsistent VQ-GAN reconstructions. Finally, we also report video prediction results for the RoboNet dataset at 256×256 resolution.

4.3 Ablation Studies

We ablate MaskViT to understand the contribution of each design decision with the default settings: 6 blocks, 768 embedding dimension, $1 \times 16 \times 16$ spatial window, $16 \times 4 \times 4$ spatiotemporal window, and variable masking ratio (Table 2).

Model hyperparameters. We compare the effect of the number of blocks and the embedding dimension in Table 2a. We find that having a larger embedding dimension improves the performance slightly, whereas increasing the number of blocks does not improve the performance.

Spatiotemporal window (STW). An important design decision of MaskViT is the size of the STW (Table 2b). We compare three different window configurations and MaskViT with full self-attention in all layers. Note that training a model with full self-attention requires using gradient checkpointing,

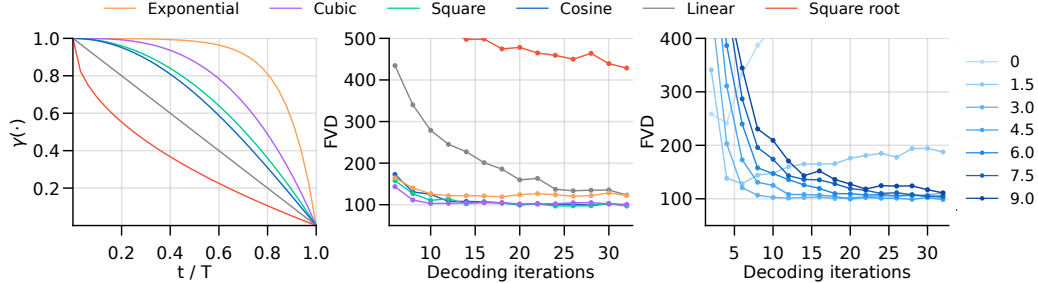


Figure 3: Mask scheduling functions. *Left:* 3 categories of mask scheduling functions: concave (cosine, square, cubic, exponential), linear, and convex (square root). *Middle:* FVD scores for different mask scheduling functions and decoding iterations. Concave functions perform the best. *Right:* FVD score vs. decoding iterations for different temperature values. Lower and higher temperature values lead to poor FVD scores, with a sweet spot temperature value of 3 and 4.5.

which significantly increases the training time. In fact, the STW size of $16 \times 4 \times 4$ achieves better accuracy, while requiring 60% less memory and speeds up training time by $3.3\times$.

Masking ratio during training. We find that a fixed masking ratio results in poor video prediction performance (Table 2c). A large masking ratio until a maximum of 95% decreases FVD. Further increase in masking ratio significantly deteriorates the performance. A *variable* masking ratio performs best, as it best approximates the different masking ratios encountered during inference.

Mask scheduling. The choice of mask scheduling function and the number of decoding iterations during inference has a significant impact on video generation quality (Fig. 3). We compare three types of scheduling functions: concave (cosine, square, cubic, exponential), linear, and convex (square root). Concave functions performed significantly better than linear and convex functions. Videos have a lot of redundant information due to temporal coherence, and consequently with only 5% of unmasked tokens (Table 2c) the entire video can be correctly predicted. The critical step is to predict these few tokens very accurately. We hypothesize that concave functions perform better as they capture this intuition by slowly predicting the initial tokens over multiple iterations and then rapidly predicting the majority of remaining tokens conditioned on the (more accurate) initial tokens in the final iterations. Convex functions operate in an opposite manner and thus perform significantly worse. Across all functions, FVD improved with increased numbers of decoding steps until a certain point. Further increasing the decoding steps did not improve FVD. Additionally, we found that selecting the most confident tokens while performing iterative decoding led to video predictions with little or no motion. Hence, we add temperature annealed Gumbel noise to the token confidence to encourage the model to produce more diverse outputs (Fig. 3). Empirically, we found that a temperature value of 4.5 works best across different datasets.

4.4 Visual Model Predictive Control with MaskViT on a Real Robot

Essential to our design is to achieve an inference performance that supports robotics and embodied AI tasks. We evaluate whether the performance improvements afforded by our method can enable the control of embodied agents through experimental evaluation on a Sawyer robot arm. We first train our model on the RoboNet dataset along with a small collection of random interaction tra-

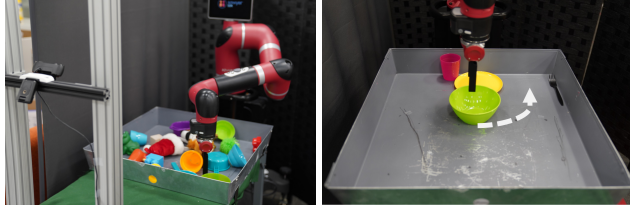


Figure 4: *Left*: Third person view of real-world data collection. *Right*: An example evaluation task. The overlaid white arrow depicts the goal location of the green bowl.

method	success rate
MaskViT (all data)	60%
MaskViT (finetuned)	53%
MaskViT (RN only)	3%
Random policy	3%

Table 4: **Control evaluation results.** We perform 30 trials for each method, and report aggregated success rates.

jectories in our setup. We then leverage MaskViT to perform visual model-predictive control, and evaluate the robot’s performance on several manipulation tasks.

Setup and data collection. We autonomously collect 120K frames of additional finetuning data from our setup to augment RoboNet. Between each pair of frames, the robot takes a 5-dimensional action representing a change in Cartesian end-effector position: $[x, y, z]$ gripper position, θ yaw angle, and a binary gripper open/close command. During data collection, the robot interacts with a diverse collection of random household objects (Fig. 4).

Model predictive control using MaskViT. We evaluate the planning capabilities of MaskViT using visual foresight [4, 5] on a series of robotic pushing tasks. Our control evaluation contains two task types: **table setting**, which involves pushing a bowl previously unseen in the training data, and **sweeping**, where objects are moved into an unseen dustpan. For each task, the robot is given a 64×64 goal image and we perform planning based on MaskViT by optimizing a sequence of actions using the cross-entropy method (CEM) [66], using the ℓ_2 pixel error between the last predicted image and the goal as the cost. We evaluate two variants of our model: one trained on the combined RoboNet and finetuning datasets (`all data`), and another that is pretrained using RoboNet and then finetuned on only the domain-specific data (`finetuned`). We compare to a baseline model trained only on RoboNet (`RN only`) as well as a random Gaussian policy. See the supplementary material for additional details and hyperparameters.

Results. As shown in Table 4, our model achieves strong planning performance when provided finetuning data, but the specific method of integrating the finetuning data (all together or post-finetuning) is not significant. We find qualitatively that a model trained only on RoboNet is unable to produce high-fidelity reconstructions of the scene, and cannot predict plausible arm motions. Critically, our method’s efficient inference procedure allows us to achieve ~ 6.5 seconds per CEM iteration, which is orders of magnitude more efficient than autoregressive models as shown in Table 3.

5 Conclusion

In this work, we explore MaskViT, a simple method for video prediction which leverages masked visual modeling as a pre-training task and transformers with window attention as a backbone for computation efficiency. We showed that by masking a *variable* number of tokens during training, we can achieve competitive video prediction results. Our iterative decoding scheme is significantly faster than autoregressive decoding and enables planning for real robot manipulation tasks.

Limitations and future work. While our results are encouraging, we found that using per frame quantization can lead to flicker artifacts, especially in videos that have a static background like RoboNet. Although MaskViT is efficient in terms of memory and parameters, scaling up video prediction, especially for scenarios that have significant camera motion (e.g., self-driving [17] and egocentric videos [67]) remains challenging. Finally, an important future avenue of exploration is scaling up the complexity of robotic tasks [68] integrating our video prediction method in more complex planning algorithms.

Acknowledgments

We thank Abhishek Kadian for helpful discussions. This work was supported by Department of Navy award (N00014-19-1-2477) issued by the Office of Naval Research and Stanford HAI. ST is supported by the NSF Graduate Research Fellowship under Grant No. DGE-1656518.

References

- [1] J. Tanji and E. V. Evarts. Anticipatory activity of motor cortex neurons in relation to direction of an intended movement. *Journal of neurophysiology*, 39(5):1062–1068, 1976.
- [2] D. M. Wolpert, Z. Ghahramani, and M. I. Jordan. An internal model for sensorimotor integration. *Science*, 269(5232):1880–1882, 1995.
- [3] T. Wu, A. J. Dufford, M.-A. Mackie, L. J. Egan, and J. Fan. The capacity of cognitive control estimated from a perceptual decision making task. *Scientific reports*, 6(1):1–11, 2016.
- [4] C. Finn and S. Levine. Deep visual foresight for planning robot motion. In *IEEE International Conference on Robotics and Automation*, 2017.
- [5] F. Ebert, C. Finn, S. Dasari, A. Xie, A. Lee, and S. Levine. Visual foresight: Model-based deep reinforcement learning for vision-based robotic control. *arXiv preprint arXiv:1812.00568*, 2018.
- [6] N. Hirose, F. Xia, R. Martín-Martín, A. Sadeghian, and S. Savarese. Deep visual mpc-policy learning for navigation. *IEEE Robotics and Automation Letters*, 4(4):3184–3191, 2019.
- [7] A. Vaswani, N. Shazeer, N. Parmar, J. Uszkoreit, L. Jones, A. N. Gomez, Ł. Kaiser, and I. Polosukhin. Attention is all you need. In *Advances in Neural Information Processing Systems*, 2017.
- [8] J. Devlin, M.-W. Chang, K. Lee, and K. Toutanova. BERT: Pre-training of deep bidirectional transformers for language understanding. In *Proceedings of the Conference of the North American Chapter of the Association for Computational Linguistics: Human Language Technologies*, 2019.
- [9] A. Van Den Oord and O. Vinyals. Neural discrete representation learning. In *Advances in Neural Information Processing Systems*, 2017.
- [10] P. Esser, R. Rombach, and B. Ommer. Taming transformers for high-resolution image synthesis. In *Proceedings of the IEEE/CVF Conference on Computer Vision and Pattern Recognition*, pages 12873–12883, 2021.
- [11] J. Sohl-Dickstein, E. Weiss, N. Maheswaranathan, and S. Ganguli. Deep unsupervised learning using nonequilibrium thermodynamics. In *International Conference on Machine Learning*, pages 2256–2265. PMLR, 2015.
- [12] J. Ho, A. Jain, and P. Abbeel. Denoising diffusion probabilistic models. *Advances in Neural Information Processing Systems*, 33:6840–6851, 2020.
- [13] A. Q. Nichol and P. Dhariwal. Improved denoising diffusion probabilistic models. In *International Conference on Machine Learning*, pages 8162–8171. PMLR, 2021.
- [14] M. Ghazvininejad, O. Levy, Y. Liu, and L. Zettlemoyer. Mask-predict: Parallel decoding of conditional masked language models. In *Proceedings of the 2019 Conference on Empirical Methods in Natural Language Processing and the 9th International Joint Conference on Natural Language Processing (EMNLP-IJCNLP)*, pages 6112–6121, Hong Kong, China, Nov. 2019. Association for Computational Linguistics. doi:[10.18653/v1/D19-1633](https://doi.org/10.18653/v1/D19-1633).

- [15] H. Chang, H. Zhang, L. Jiang, C. Liu, and W. T. Freeman. Maskgit: Masked generative image transformer. *arXiv preprint arXiv:2202.04200*, 2022.
- [16] F. Ebert, C. Finn, A. X. Lee, and S. Levine. Self-supervised visual planning with temporal skip connections. In *Conference on Robot Learning*, pages 344–356, 2017.
- [17] A. Geiger, P. Lenz, C. Stiller, and R. Urtasun. Vision meets robotics: The kitti dataset. *The International Journal of Robotics Research*, 32(11):1231–1237, 2013.
- [18] S. Dasari, F. Ebert, S. Tian, S. Nair, B. Bucher, K. Schmeckpeper, S. Singh, S. Levine, and C. Finn. Robonet: Large-scale multi-robot learning. *arXiv preprint arXiv:1910.11215*, 2019.
- [19] M. Ranzato, A. Szlam, J. Bruna, M. Mathieu, R. Collobert, and S. Chopra. Video (language) modeling: a baseline for generative models of natural videos. *arXiv preprint arXiv:1412.6604*, 2014.
- [20] W. Lotter, G. Kreiman, and D. Cox. Deep predictive coding networks for video prediction and unsupervised learning. *arXiv preprint arXiv:1605.08104*, 2016.
- [21] Y. Li, M. Min, D. Shen, D. Carlson, and L. Carin. Video generation from text. In *Proceedings of the AAAI Conference on Artificial Intelligence*, 2018.
- [22] T. Gupta, D. Schwenk, A. Farhadi, D. Hoiem, and A. Kembhavi. Imagine this! scripts to compositions to videos. In *Proceedings of the European Conference on Computer Vision (ECCV)*, pages 598–613, 2018.
- [23] Y. Pan, Z. Qiu, T. Yao, H. Li, and T. Mei. To create what you tell: Generating videos from captions. In *Proceedings of the 25th ACM International Conference on Multimedia*, pages 1789–1798, 2017.
- [24] C. Wu, J. Liang, L. Ji, F. Yang, Y. Fang, D. Jiang, and N. Duan. NUWA: Visual synthesis pre-training for neural visual world creation. *arXiv preprint arXiv:2111.12417*, 2021.
- [25] C. Finn, I. Goodfellow, and S. Levine. Unsupervised learning for physical interaction through video prediction. In *Advances in Neural Information Processing Systems*, 2016.
- [26] R. Villegas, A. Pathak, H. Kannan, D. Erhan, Q. V. Le, and H. Lee. High fidelity video prediction with large stochastic recurrent neural networks. *Advances in Neural Information Processing Systems*, 32, 2019.
- [27] B. Wu, S. Nair, R. Martin-Martin, L. Fei-Fei, and C. Finn. Greedy hierarchical variational autoencoders for large-scale video prediction. In *Proceedings of the IEEE/CVF Conference on Computer Vision and Pattern Recognition*, pages 2318–2328, 2021.
- [28] M. Babaeizadeh, M. T. Saffar, S. Nair, S. Levine, C. Finn, and D. Erhan. Fitvid: Overfitting in pixel-level video prediction. *arXiv preprint arXiv:2106.13195*, 2021.
- [29] A. Clark, J. Donahue, and K. Simonyan. Adversarial video generation on complex datasets. *arXiv preprint arXiv:1907.06571*, 2019.
- [30] S. Tulyakov, M.-Y. Liu, X. Yang, and J. Kautz. Mocogan: Decomposing motion and content for video generation. In *Proceedings of the IEEE Conference on Computer Vision and Pattern Recognition*, pages 1526–1535, 2018.
- [31] P. Luc, A. Clark, S. Dieleman, D. d. L. Casas, Y. Doron, A. Cassirer, and K. Simonyan. Transformation-based adversarial video prediction on large-scale data. *arXiv preprint arXiv:2003.04035*, 2020.
- [32] M. Babaeizadeh, C. Finn, D. Erhan, R. H. Campbell, and S. Levine. Stochastic variational video prediction. In *International Conference on Learning Representations*, 2018.

- [33] E. Denton and R. Fergus. Stochastic video generation with a learned prior. In *International Conference on Machine Learning*, pages 1174–1183. PMLR, 2018.
- [34] A. K. Akan, E. Erdem, A. Erdem, and F. Güney. Slamp: Stochastic latent appearance and motion prediction. In *Proceedings of the IEEE/CVF International Conference on Computer Vision*, pages 14728–14737, 2021.
- [35] A. K. Akan, S. Safadoust, E. Erdem, A. Erdem, and F. Güney. Stochastic video prediction with structure and motion. *arXiv preprint arXiv:2203.10528*, 2022.
- [36] M. Dorkenwald, T. Milbich, A. Blattmann, R. Rombach, K. G. Derpanis, and B. Ommer. Stochastic image-to-video synthesis using cinns. In *Proceedings of the IEEE/CVF Conference on Computer Vision and Pattern Recognition*, pages 3742–3753, 2021.
- [37] W. Yan, Y. Zhang, P. Abbeel, and A. Srinivas. Videogpt: Video generation using vq-vae and transformers. *arXiv preprint arXiv:2104.10157*, 2021.
- [38] R. Rakhimov, D. Volkhonskiy, A. Artemov, D. Zorin, and E. Burnaev. Latent video transformer. *arXiv preprint arXiv:2006.10704*, 2020.
- [39] C. Nash, J. Carreira, J. Walker, I. Barr, A. Jaegle, M. Malinowski, and P. Battaglia. Transframer: Arbitrary frame prediction with generative models. *arXiv preprint arXiv:2203.09494*, 2022.
- [40] J. Ho, T. Salimans, A. Gritsenko, W. Chan, M. Norouzi, and D. J. Fleet. Video diffusion models. *arXiv preprint arXiv:2204.03458*, 2022.
- [41] V. Voleti, A. Jolicoeur-Martineau, and C. Pal. Masked conditional video diffusion for prediction, generation, and interpolation. *arXiv preprint arXiv:2205.09853*, 2022.
- [42] P. Vincent, H. Larochelle, Y. Bengio, and P.-A. Manzagol. Extracting and composing robust features with denoising autoencoders. In *Proceedings of the 25th International Conference on Machine Learning*, pages 1096–1103, 2008.
- [43] T. Brown, B. Mann, N. Ryder, M. Subbiah, J. D. Kaplan, P. Dhariwal, A. Neelakantan, P. Shyam, G. Sastry, A. Askell, et al. Language models are few-shot learners. In *Advances in Neural Information Processing Systems*, 2020.
- [44] A. Radford, J. Wu, R. Child, D. Luan, D. Amodei, I. Sutskever, et al. Language models are unsupervised multitask learners. *OpenAI blog*, 1(8):9, 2019.
- [45] K. He, X. Chen, S. Xie, Y. Li, P. Dollár, and R. Girshick. Masked autoencoders are scalable vision learners. *arXiv preprint arXiv:2111.06377*, 2021.
- [46] A. Dosovitskiy, L. Beyer, A. Kolesnikov, D. Weissenborn, X. Zhai, T. Unterthiner, M. Dehghani, M. Minderer, G. Heigold, S. Gelly, et al. An image is worth 16x16 words: Transformers for image recognition at scale. *arXiv preprint arXiv:2010.11929*, 2020.
- [47] H. Bao, L. Dong, S. Piao, and F. Wei. BEit: BERT pre-training of image transformers. In *International Conference on Learning Representations*, 2022.
- [48] M. Chen, A. Radford, R. Child, J. Wu, H. Jun, D. Luan, and I. Sutskever. Generative pretraining from pixels. In *International Conference on Machine Learning*, pages 1691–1703. PMLR, 2020.
- [49] Z. Tong, Y. Song, J. Wang, and L. Wang. Videomae: Masked autoencoders are data-efficient learners for self-supervised video pre-training. *arXiv preprint arXiv:2203.12602*, 2022.
- [50] C. Feichtenhofer, H. Fan, Y. Li, and K. He. Masked autoencoders as spatiotemporal learners. *arXiv preprint arXiv:2205.09113*, 2022.

- [51] M. Laskin, A. Srinivas, and P. Abbeel. CURL: Contrastive unsupervised representations for reinforcement learning. In H. D. III and A. Singh, editors, *Proceedings of the 37th International Conference on Machine Learning*, volume 119 of *Proceedings of Machine Learning Research*, pages 5639–5650. PMLR, 13–18 Jul 2020.
- [52] S. Nair, A. Rajeswaran, V. Kumar, C. Finn, and A. Gupta. R3m: A universal visual representation for robot manipulation. *arXiv preprint arXiv:2203.12601*, 2022.
- [53] S. Parisi, A. Rajeswaran, S. Purushwalkam, and A. Gupta. The unsurprising effectiveness of pre-trained vision models for control. *arXiv preprint arXiv:2203.03580*, 2022.
- [54] T. Xiao, I. Radosavovic, T. Darrell, and J. Malik. Masked visual pre-training for motor control. *arXiv preprint arXiv:2203.06173*, 2022.
- [55] A. Razavi, A. Van den Oord, and O. Vinyals. Generating diverse high-fidelity images with vq-vae-2. In *Advances in Neural Information Processing Systems*, 2019.
- [56] I. Goodfellow, J. Pouget-Abadie, M. Mirza, B. Xu, D. Warde-Farley, S. Ozair, A. Courville, and Y. Bengio. Generative adversarial nets. In *Advances in Neural Information Processing Systems*, 2014.
- [57] J. Johnson, A. Alahi, and L. Fei-Fei. Perceptual losses for real-time style transfer and super-resolution. In *European Conference on Computer Vision*, pages 694–711. Springer, 2016.
- [58] R. Zhang, P. Isola, A. A. Efros, E. Shechtman, and O. Wang. The unreasonable effectiveness of deep features as a perceptual metric. In *Proceedings of the IEEE Conference on Computer Vision and Pattern Recognition*, pages 586–595, 2018.
- [59] Z. Liu, Y. Lin, Y. Cao, H. Hu, Y. Wei, Z. Zhang, S. Lin, and B. Guo. Swin transformer: Hierarchical vision transformer using shifted windows. In *Proceedings of the IEEE/CVF International Conference on Computer Vision*, pages 10012–10022, 2021.
- [60] Z. Liu, J. Ning, Y. Cao, Y. Wei, Z. Zhang, S. Lin, and H. Hu. Video swin transformer. *arXiv preprint arXiv:2106.13230*, 2021.
- [61] R. Child, S. Gray, A. Radford, and I. Sutskever. Generating long sequences with sparse transformers. *arXiv preprint arXiv:1904.10509*, 2019.
- [62] A. X. Lee, R. Zhang, F. Ebert, P. Abbeel, C. Finn, and S. Levine. Stochastic adversarial video prediction. *arXiv preprint arXiv:1804.01523*, 2018.
- [63] D. Weissenborn, O. Täckström, and J. Uszkoreit. Scaling autoregressive video models. In *International Conference on Learning Representations*, 2020.
- [64] T. Unterthiner, S. van Steenkiste, K. Kurach, R. Marinier, M. Michalski, and S. Gelly. Towards accurate generative models of video: A new metric & challenges. *arXiv preprint arXiv:1812.01717*, 2018.
- [65] Z. Wang, A. C. Bovik, H. R. Sheikh, and E. P. Simoncelli. Image quality assessment: from error visibility to structural similarity. *IEEE Transactions on Image Processing*, 13(4):600–612, 2004.
- [66] P. D. Boer, Kroese, S. Mannor, and R. Y. Rubinstein. A tutorial on the cross-entropy method. *Annals of Operations Research*, 134(1):19–67, 2004.
- [67] K. Grauman, A. Westbury, E. Byrne, Z. Chavis, A. Furnari, R. Girdhar, J. Hamburger, H. Jiang, M. Liu, X. Liu, et al. Ego4d: Around the world in 3,000 hours of egocentric video. *arXiv preprint arXiv:2110.07058*, 3, 2021.

- [68] S. Srivastava, C. Li, M. Lingelbach, R. Martín-Martín, F. Xia, K. E. Vainio, Z. Lian, C. Gokmen, S. Buch, K. Liu, et al. Behavior: Benchmark for everyday household activities in virtual, interactive, and ecological environments. In *Conference on Robot Learning*, pages 477–490. PMLR, 2022.
- [69] D. P. Kingma and J. Ba. Adam: A method for stochastic optimization. In *ICLR (Poster)*, 2015.
URL <http://arxiv.org/abs/1412.6980>.
- [70] P. Goyal, P. Dollár, R. Girshick, P. Noordhuis, L. Wesolowski, A. Kyrola, A. Tulloch, Y. Jia, and K. He. Accurate, large minibatch sgd: Training imagenet in 1 hour. *arXiv preprint arXiv:1706.02677*, 2017.
- [71] P.-T. De Boer, D. P. Kroese, S. Mannor, and R. Y. Rubinstein. A tutorial on the cross-entropy method. *Annals of operations research*, 134(1):19–67, 2005.
- [72] A. Nagabandi, K. Konoglie, S. Levine, and V. Kumar. Deep Dynamics Models for Learning Dexterous Manipulation. In *Conference on Robot Learning (CoRL)*, 2019.

A Implementation Details

A.1 Training MaskViT

VQ-GAN. We train a VQ-GAN [10] model for each dataset which downsamples each frame into 16×16 latent codes, i.e., by a factor of 4 for frames of size 64×64 frames and 16 for frames of size 256×256 . Table 5 summarizes our settings for all three datasets. Training VQ-GAN with discriminator loss can lead to instabilities. Hence, as suggested by [10] we start GAN losses after the reconstruction loss has converged. We also found that GAN losses were not always helpful, especially at lower input resolutions for BAIR and RoboNet.

Transformer. Our transformer model is a stack of L blocks, where each block consists of two transformer layers with attention restricted to the window size of $1 \times 16 \times 16$ (spatial window) and $T \times 4 \times 4$ (spatiotemporal window), unless otherwise specified. We use learnable positional embeddings, which are the sum of space and time positional embeddings. Following [59], we adopt relative position biases in our layers. We use the Adam [69] optimizer with linear warmup [70] and a cosine decay learning rate schedule. Table 5 summarizes our settings for all three datasets.

Evaluation. We find the optimal evaluation parameters by doing a grid search of the following parameters: γ (cosine, square), temperature (3, 4.5) and decoding iterations depending on the prediction horizon length. We use top-p value of 0.95 for the BAIR dataset only. Table 5 summarizes our evaluation settings.

Dataset	BAIR	KITTI	KITTI	RoboNet	RoboNet
Image resolution	64	64	256	64	256
Context frames	1	5	5	2	2
<hr/>					
VQ-GAN					
Channel	160	128	128	192	128
K	1024	1024	1024	1024	1024
n_z	256	256	256	256	256
Batch size	320	1120	112	720	112
Training steps	3e5	5e4	3e5	3e5	3e5
Learning rate	1e-4	1e-3	1e-4	5e-4	1e-4
Disc. start	-	2e4	1.5e5	-	1.5e5
<hr/>					
Transformer					
Spatial window	$1 \times 16 \times 16$				
Spatiotemporal window	$16 \times 8 \times 8$	$16 \times 4 \times 4$			
Blocks	6	8	6	8	6
Attention heads	4	4	4	4	4
Embedding dim.	768	768	1024	768	1024
Feedforward dim.	3072	3072	4096	3072	4096
Dropout	0.0	0.0	0.0	0.0	0.0
Batch size	64	32	32	224	224
Learning rate	3e-4	3e-4	3e-4	3e-4	3e-4
Training steps	1e5	1e5	1e5	3e5	3e5
<hr/>					
Evaluation					
Mask scheduling func.	square	cosine	cosine	cosine	cosine
Decoding iters.	18	48	64	7	16
Temperature	4.5	3.0	4.5	-	-

Table 5: **Training and evaluation hyperparameters.**

A.2 Real Robot Experiments

Data collection. Our robot setup consists of a Sawyer robot arm with a Logitech C922 PRO consumer webcam for recording video frames at 640×480 resolution. All raw image observations are center-cropped to 480×480 resolution before being resized to 64×64 for model training and control in our experiments. We autonomously collect 4000 trajectories of 30 timesteps. At each step the robot takes a 5-dimensional action representing a change in state of the end-effector: a delta translation in Cartesian space, $[x, y, z]$, for the gripper position in meters, change in θ yaw angle of the end-effector, and a binary gripper open/close command. Following the action space used to collect the RoboNet dataset, the pitch and roll of the end-effector are kept fixed such that the gripper points with the fingers towards the table surface. Each action within a trajectory is selected independently and each dimension of the action vector is independent of the others, sampled from a diagonal Gaussian distribution, except the gripper open/close command that closes automatically when the z -position of the end-effector reaches below a certain threshold to increase the rate of object interaction. The random action distribution is parameterized by $\mathcal{N}(0, \text{diag}([0.035, 0.035, 0.08, \pi/18, 2]))$. During data collection, we provide the robot with a diverse set of training objects to interact with. During evaluation, we test on tasks which require the robot to manipulate unseen bowls in one setting and to push training items into an unseen dustpan in another.

Visual-MPC. Our control strategy is a visual MPC [4, 5] procedure. Given a start and goal image $I_0, I_g \in \mathbb{R}^{64 \times 64 \times 3}$, the objective is to find an optimal sequence of actions to reach the goal observation from the start. The planning objective can be written as: $\min_{a_1, a_2, \dots, a_H} \sum_{i=1}^H c_i \|\hat{f}(I_0, a_1, \dots, a_H)_i - I_g\|_2^2$, where $\hat{f}(I_0, a_1, \dots, a_H)_i$ represents the i th predicted frame by the learned video prediction model (MaskViT in our case), and c_i are a sequence of constant hyperparameters that determine the importance of the difference between the predicted frame and the goal for each time step.

We use the cross-entropy method (CEM) [71] to optimize a sequence of $H = 10$ future actions for this objective. In each planning iteration, we first sample $M = 256$ sequences of random actions. We then provide these sequences, together with two consecutive context frames (the previous and current step observations), and one context action (the action taken at the previous step) to MaskViT. Action sequences are sampled according to a multivariate Gaussian distribution. To bias action sampling towards smoother trajectories, the noise samples for actions in a given random trajectory are correlated across time as in Nagabandi et al. [72]. Specifically, given a correlation coefficient hyperparameter β , we first compute $u_i^1, u_i^2, \dots, u_i^M \stackrel{i.i.d.}{\sim} N(0, \Sigma_i)$, where Σ_i is the variance of the action at timestep i in the current optimization iteration. The noise at timestep i for the j th random trajectory, n_i^j , is then computed as a weighted combination of the new noise sample and the noise sample at the previous timestep, that is, $n_i^j = (1 - \beta) * u_i^j + \beta * n_{i-1}^j$. After all noise samples are computed, they are summed with means μ_i for each timestep, which are also iteratively updated. The final random trajectories are formed by rounding the elements in the last action dimension (gripper action) to -1 or 1 , whichever is closer.

Next, we compare the predictions to the goal image by computing the ℓ_2 error and summing over time as described by the objective above. We weight the cost on the final timestep by $10\times$, but still include the costs on intermediate timesteps in the summation to encourage the robot to solve the task quickly. The best action sequences based on this score are used to refit the sampling distribution mean and variance for the next optimization iteration. After $K = 3$ optimization iterations, we execute the best scoring action sequence on the robot for the first 3 steps before performing replanning.

The robot uses a total of 15 steps to solve the task, including one initial action = $[0, 0, -0.08, 0.1, 0]$ which is executed at the beginning of every trajectory. This ensures that at least two context images provided for planning. The planning hyperparameters are summarized in Table 6.

Evaluation. We perform control evaluation on two categories of tasks: table setting and sweeping. For each task, we test 5 different variations with 3 trials each. A trial is considered successful if the center of the object of interest is within 8 cm of the goal position after the trajectory

is complete. Model inference for real robot control is performed using 8 NVIDIA RTX 3090 GPUs with a batch size of 16 per GPU. We use 5 decoding iterations, which yields a forward pass time of approximately 6.2 seconds for a batch of 256 samples.

Hyperparameter	Value
Total trajectory length (T)	15
Planning horizon	10
Number of steps between replanning	3
Action dimension	5
# of samples per CEM iteration (M)	256
# of CEM iterations (K)	3
Weights on each timestep in cost (c_i)	1 if $i = 0, \dots, 8$; 10 if $i = 9$
Initial sampling distribution mean	$[0, 0, -0.5, 0, 0]$
Initial sample distribution std.	$[0.05, 0.05, 0.08, \pi/18, 2]$
Sampled noise correlation coefficient (β)	0.3
CEM fraction of elites	0.05
MaskViT mask scheduling function	Cosine
MaskViT decoding iterations	5

Table 6: **Hyperparameters for visual-MPC.**

B Additional Results

B.1 Qualitative Results

Video prediction. We present additional qualitative video prediction results for BAIR (Fig. 7), KITTI (Fig. 8) and RoboNet (Fig. 9).

Real robot experiments. Fig. 5 and Fig. 6 depict sample predictions for MaskViT (all data) and MaskViT trained only on RoboNet (RN only) for two example control tasks. We observe that with our model, the planner is able to find sequences of actions which bring the blue bowl or the soft red hat close to the position specified in the goal image. However, with a model which is trained only on the RoboNet dataset, planning fails. We see qualitatively that the model trained in RoboNet-only, even when solely performing reconstruction of the first two context images using the VQ-GAN component, is unable to reconstruct the background and robot arm with high fidelity. Despite the diversity of the RoboNet dataset, finetuning on domain-specific data is still required to produce reasonable predictions in our setting.

B.2 Quantitative Results

Real robot experiments. Table 7 shows per-task success rates for our real-world robotic control evaluation. Each of our two task types (table setting, sweeping) has 5 variations, each of which involves different objects to push (unseen bowls for table setting, toys previously seen in the finetuning data for sweeping) and different target locations.

Task	MaskViT (all data)	MaskViT (finetuned)	MaskViT (RN only)	Random
<i>table setting (bowl color; destination)</i>				
blue; front-left	2/3	1/3	0/3	0/3
green; back-right	0/3	0/3	0/3	0/3
blue; front-right	2/3	2/3	1/3	0/3
red; front	3/3	2/3	0/3	0/3
green; left	2/3	3/3	0/3	0/3
<i>sweeping (object; destination)</i>				
toys; back-right	3/3	3/3	0/3	0/3
hat; front-right	1/3	2/3	0/3	0/3
hat; front-left	2/3	1/3	0/3	1/3
toys; back-left	1/3	1/3	0/3	0/3
toys; front-left	2/3	1/3	0/3	0/3
Aggregated	18/30	16/30	1/30	1/30

Table 7: **Per-task quantitative results** for our robotic control evaluation. We evaluate each of 5 variants of the two tasks using 3 trials with each model or policy. Success is determined by the center of the object being within 8cm of the goal position at the end of 15 steps.



Figure 5: Visualizations for task set table: push blue bowl left.

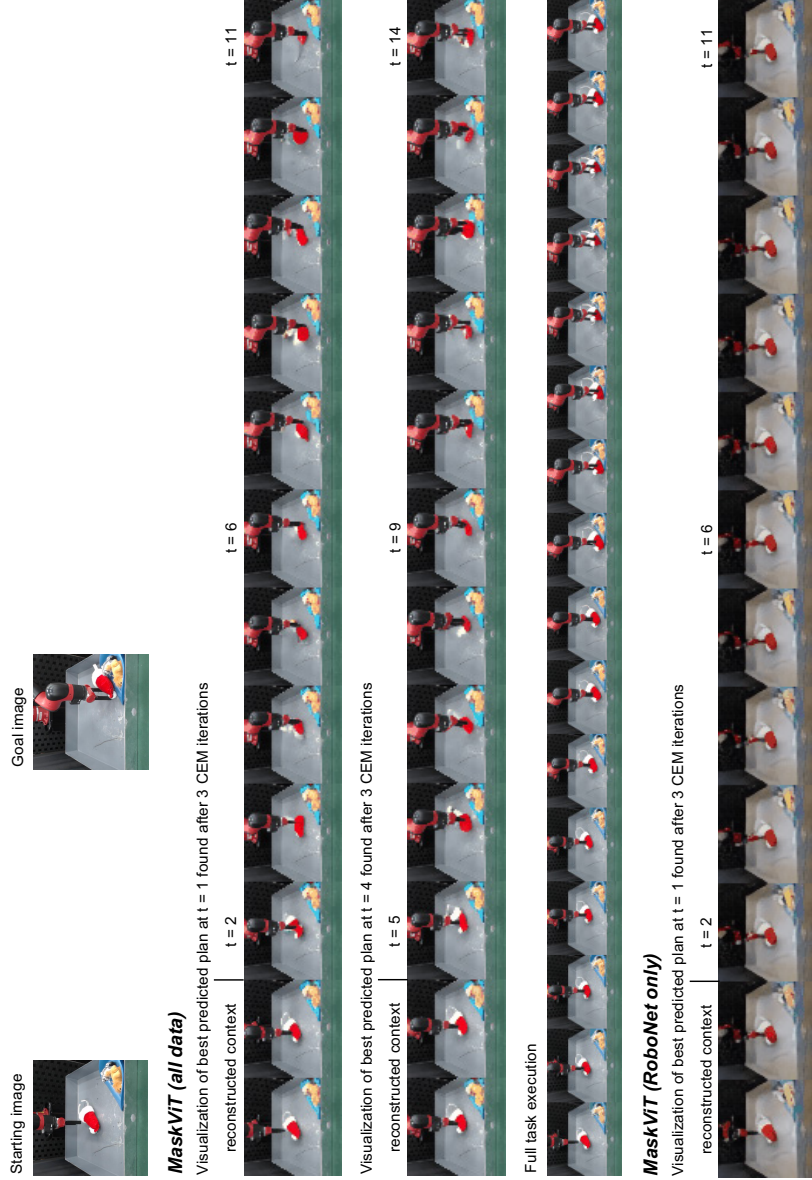


Figure 6: Visualizations for task sweep: push hat to bottom-right corner.



Figure 7: Qualitative results: BAIR (action free, 64×64)

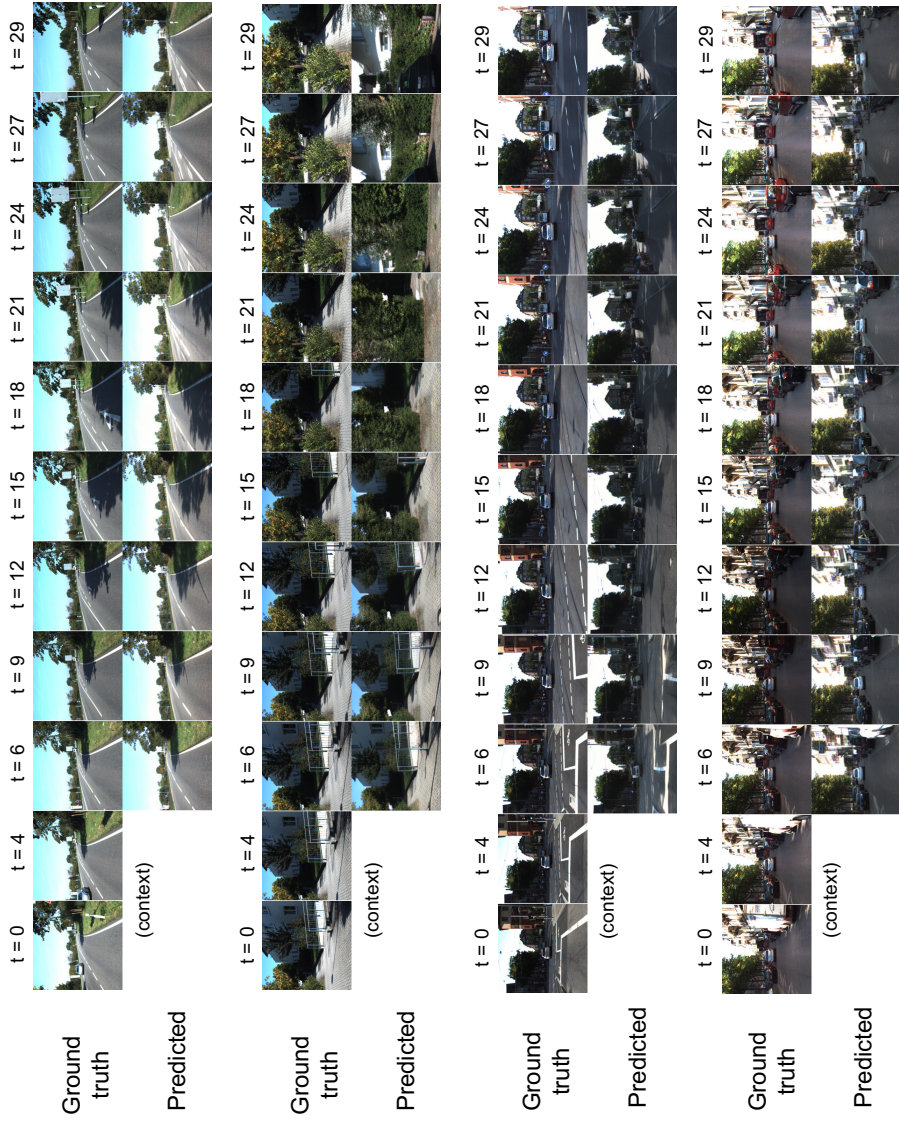


Figure 8: Qualitative results: KITTI (256×256)

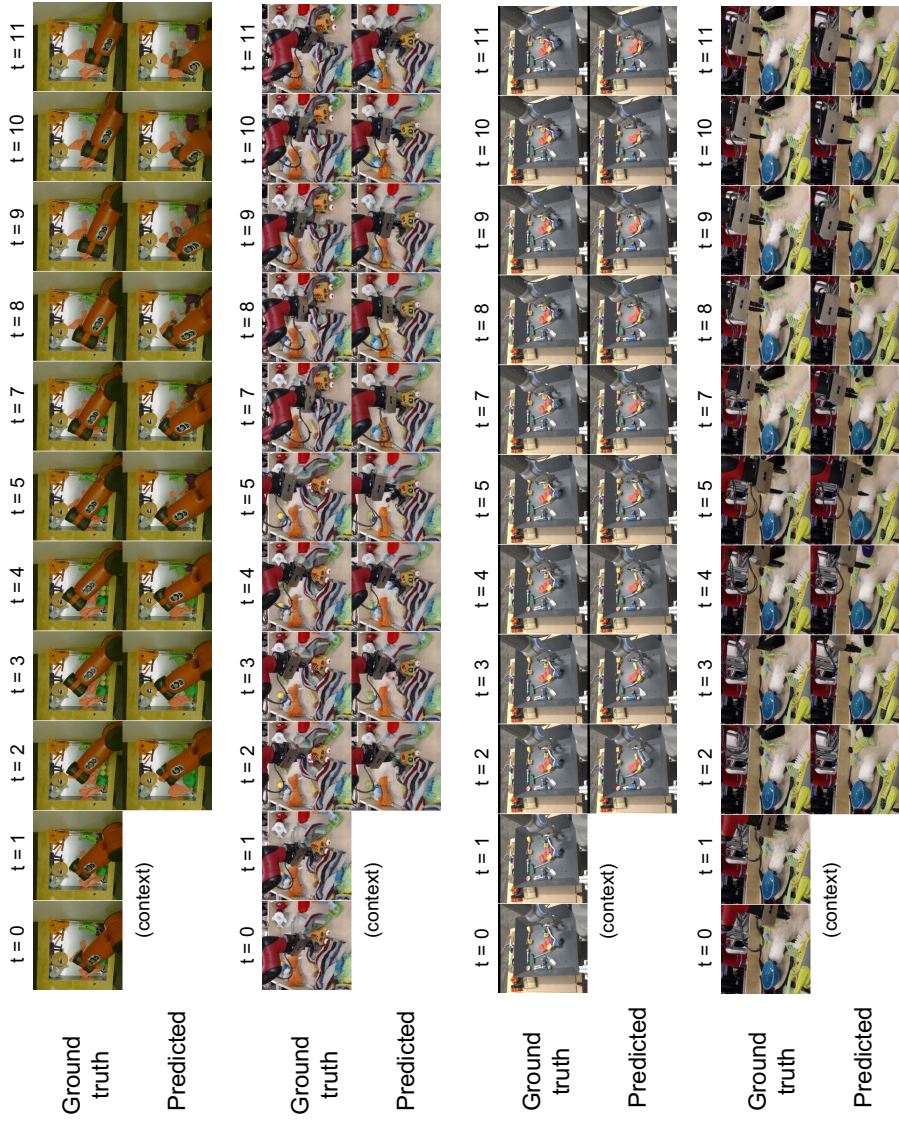


Figure 9: Qualitative results: RoboNet (256×256)